Impact of a small number of nonmagnetic impurities on *H-T* magnetic phase diagram of $CuFeO_2$

Noriki Terada* and Setsuo Mitsuda
Department of Physics, Faculty of Science, Tokyo University of Science, Kagurazaka 1-3, Shinjuku-ku, Tokyo, Japan

Karel Prokes
Hahn-Meitner-Institute, Glienicker Strasse 100, D-14109 Berlin, Germany

Osamu Suzuki and Hideaki Kitazawa
Nanomaterials Laboratory, National Institute for Materials Science, Tsukuba-shi, Ibaraki 305-0047, Japan

H. Aruga Katori
RIKEN (The Institute of Physical and Chemical Research) Wako, Saitama 351-0198, Japan
(Received 15 July 2003; revised manuscript received 16 July 2004; published 11 November 2004)

We have obtained the magnetic field (H) versus temperature (T) magnetic phase diagram for the triangular lattice antiferromagnet $CuFe_{0.98}Al_{0.02}O_2$ using neutron diffraction, magnetization and specific heat measurements on single-crystal samples. On the substitution of a small amount of nonmagnetic Al^{3+} impurity for Fe^{3+}, the *H-T* phase diagram was completely modified from that of $CuFeO_2$, suggesting that the quasi-Ising spin character observed in $CuFeO_2$ disappears, and the Heisenberg spin character of Fe^{3+} is retrieved as a result of the substitution.

DOI: 10.1103/PhysRevB.70.174412 PACS number(s): 75.25.+z, 75.30.Kz, 75.50.Ee, 75.60.Ej

I. INTRODUCTION

ABO_2-type compounds with the delafossite structure represent a good example of triangular lattice antiferromagnets (TLA), and present an opportunity to study the influence of geometrical spin frustration in magnetic systems. Unlike the well-studied quasi-one-dimensional ABX_3-type hexagonal antiferromagnets,[1] ABO_2-type materials have a triangular lattice layered structure in which each triangular lattice layer is stacked rhombohedrally along the hexagonal c axis.

$CuFeO_2$ has been extensively investigated as one of the TLA ABO_2-type materials.[2–14] In spite of the Heisenberg character of the orbital singlet Fe^{3+} $\left(S=\frac{5}{2},\ L=0\right)$ magnetic ions, $CuFeO_2$ shows a quasi-Ising character: As the ground state, the four-sublattice ($\uparrow\uparrow\downarrow\downarrow$) magnetic structure with collinear magnetic moments along the c axis is realized. This is in contrast to the noncollinear 120° magnetic structure of a typical Heisenberg spin TLA. With increasing temperature, in a zero magnetic field, a quasi-long range ordered sinusoidally amplitude-modulated state is thermally induced from the ground state as a partially disordered (PD) state characteristic of an Ising spin TLA.[8] When a magnetic field is applied along the c axis at low temperatures, $CuFeO_2$ shows multi-step meta-magnetic phase transitions.[3,9] It should be emphasized that this quasi-Ising character of $CuFeO_2$ cannot be explained by typical Heisenberg spin TLA models. In contrast, the magnetic properties of other ABO_2-type TLA materials, such as $LiCrO_2$, $CuCrO_2$ and $AgCrO_2$, can be satisfactorily explained by the typical Heisenberg spin TLA model.[1]

Recently, in order to understand the stability of the quasi-Ising character, we investigated magnetic ordering in $CuFe_{1-x}Al_xO_2$ by neutron diffraction, magnetic susceptibility and specific heat measurements using single-crystal samples, with $x=0.02$ and $x=0.05$ in a zero magnetic field.[15] The results for both samples suggested that the quasi-Ising character seen in $CuFeO_2$ disappears, and the Heisenberg spin character of orbital singlet Fe^{3+} appears, because of the disturbance of the delicate balance between the competing exchange interactions in $CuFeO_2$. In the case of the $x=0.05$ sample, the lower magnetic phase transition temperature could not be found down to 2 K, although the upper transition temperature remained almost unchanged with respect to that of $CuFeO_2$. This suggests that the disruption of some part of the exchange interactions is so great that successive magnetic phase transitions disappear. On the other hand, for the $x=0.02$ sample, successive magnetic phase transitions remain. They are, however, entirely modified with respect to the transitions seen for $CuFeO_2$. Considering the significant modification of the successive magnetic phase transitions in the $x=0.02$ sample in a zero magnetic field,[15] we anticipated that the *H-T* magnetic phase diagram of $CuFeO_2$ should be also modified significantly.

To explore how the *H-T* magnetic phase diagram of $CuFeO_2$ (see Ref. 12) is modified by the substitution of a small amount of nonmagnetic impurity, in the present study, we have performed neutron diffraction, magnetization and specific heat measurements using single-crystal $CuFe_{0.98}Al_{0.02}O_2$ specimens.

II. EXPERIMENTAL DETAILS

Single-crystal material with a nominal composition of $CuFe_{0.98}Al_{0.02}O_2$ was prepared by the floating zone technique.[16] All the single-crystal samples used in this study for the neutron diffraction, magnetization and specific heat

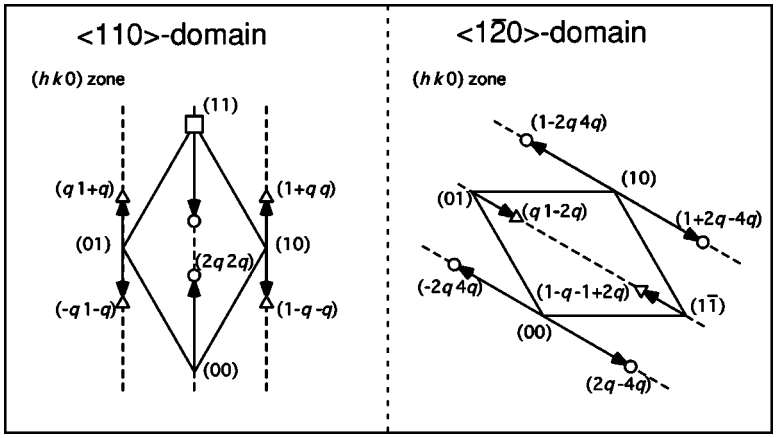

FIG. 1. Schematic drawings of the reciprocal lattice zone for the magnetic domains with the propagation wave vector along the $\langle 110 \rangle$ or the $\langle 1\bar{2}0 \rangle$ direction. The positions of the $2q$ reflections and the q reflections for the magnetically ordered states are shown by circle and triangle symbols, respectively. The square symbol shows the nuclear peak position.

measurements were obtained from identical grown rods used in the zero-field experiments.[15]

For the neutron diffraction experiments, we used the two-axis diffractometer E4 at the Berlin Neutron Scattering Center of the Hahn–Meitner Institut. The single-crystal sample was mounted in a 14.5 T vertical field cryomagnet VM-1 with its c axis vertical, to provide access to the hexagonal $(hk0)$ reciprocal lattice zone. Therefore, the spin density projected on the basal c plane could be surveyed. A magnetic field was applied along the hexagonal c axis. Whereas the reflections with the fundamental wave number q, the *q reflections*, were observed in the previous zero-field diffraction experiments[15] with a $(hh\ell)$ zone, in the present study with the $(hk0)$ zone, higher-order harmonic reflections, such as the $2q$ reflection or $4q$ reflection, can be observed at the reciprocal lattice positions denoted by circles in Fig. 1. This is because the spin density modulated along the hexagonal $\langle 1\ 1\ 0 \rangle$ direction is stacked antiferromagnetically along the c axis, as was shown in our previous work[12] on $CuFeO_2$ [see Figs. 3(c) and 5 in Ref. 12]. In addition to these higher-order reflections, weak but measurable q reflections were also observed at the positions denoted by triangles in Fig. 1, owing to stacking faults along the c axis in this sample. It should be noted that we confirmed that the $2q$ reflections at the equivalent positions reflecting the hexagonal three-fold symmetry have almost equal intensities with each other within experimental accuracy. In the case of the q reflections, since the $(1-q\ -1+2q\ 0)$ reflection in the $\langle 1\bar{2}0 \rangle$ domain was the largest in several observed q-reflections, we concentrated on surveying $\langle 1\bar{2}0 \rangle$ domain (not $\langle 110 \rangle$ domain) for the investigation of the q reflection. An incident neutron wavelength of $\lambda = 2.44$ Å was obtained using pyrolytic graphite (PG) monochromators. To suppress higher-order contaminations, a PG filter was used. A collimation of 40′-40′-40′ was employed.

For magnetization measurements, we used the extraction method ($2\ \mathrm{K} \leqslant T \leqslant 20\ \mathrm{K}, 0\ \mathrm{T} \leqslant H \leqslant 15\ \mathrm{T}$) and a Quantum Design superconducting quantum interference device magnetometer ($2\ \mathrm{K} \leqslant T \leqslant 20\ \mathrm{K},\ 0\ \mathrm{T} \leqslant H \leqslant 5\ \mathrm{T}$). For specific heat measurements, we used an Oxford instruments MagLab^{HC} microcalorimeter ($0.6\ \mathrm{K} \leqslant T \leqslant 20\ \mathrm{K},\ 0\ \mathrm{T} \leqslant H \leqslant 12\ \mathrm{T}$). For the magnetization and the specific heat measurements, a magnetic field was also applied along the c axis. The c axis of the samples was aligned with the magnetic field within ±2°. For all the scans with increasing temperatures and magnetic field, zero-field cooling procedure was used.

III. EXPERIMENTAL RESULTS

The anomalies observed in the magnetization, specific heat and neutron diffraction measurements are shown in the H-T phase diagram for $CuFe_{0.98}Al_{0.02}O_2$ in Fig. 2(b). The three magnetically ordered states are the intermediate-temperature (IM) state, the low-temperature (LT) state and the field-induced (FI) state. The shape of the H-T phase diagram for $CuFeO_2$ (see Ref. 12) shown in Fig. 2(a) is entirely modified as a result of the substitution of a small amount of nonmagnetic Al^{3+} impurity for Fe^{3+}, as seen in Fig. 2(b). The magnetic field variation of T_{N1}, $T_{N1}(H)$, remains almost unchanged from $T_{N1}^{x=0.00}(H)$; in contrast, the field variation of the lower transition temperature is completely changed. Note that the notation $T_{N1}(H)$ indicates the transition temperatures of $CuFe_{0.98}Al_{0.02}O_2$ unless specified, and the notation $T_{N1}^{x=0.00}(H)$ and $T_{N2}^{x=0.00}(H)$ stand for the transition temperatures of $CuFeO_2$. It should be particularly emphasized that the character of the triple point, where the three magnetic states meet, differs between the samples. The three phase boundaries of $CuFeO_2$ separating the four-sublattice state, the five-sublattice-like state and the PD state meet with "zero angle." In contrast, those of $CuFe_{0.98}Al_{0.02}O_2$ separating the LT state, the FI state and the IM state meet with a "finite angle." This suggests that the substitution of a small amount of nonmagnetic impurity modifies the thermodynamic properties of $CuFeO_2$. In the following sections, we will discuss the experimental results that were used to determine the magnetically ordered states and the magnetic phase boundaries.

A. Magnetization curves at low temperatures

The magnetization curve for $CuFeO_2$ exhibits magnetization plateaus in the four-sublattice state ($0\ \mathrm{T} \leqslant H \leqslant 7\ \mathrm{T}$) and the five-sublattice state ($13\ \mathrm{T} \leqslant H \leqslant 20\ \mathrm{T}$) with collinear magnetic structure,[12] as shown by the open symbols in Fig. 3(a), reflecting a strong Ising anisotropy. On the other hand, a linear increment with a finite gradient is seen in the magnetization curve of the five-sublattice-like state ($7\ \mathrm{T} \leqslant H \leqslant 13\ \mathrm{T}$), implying that the spin orientation continuously changes with varying magnetic field. This agrees with

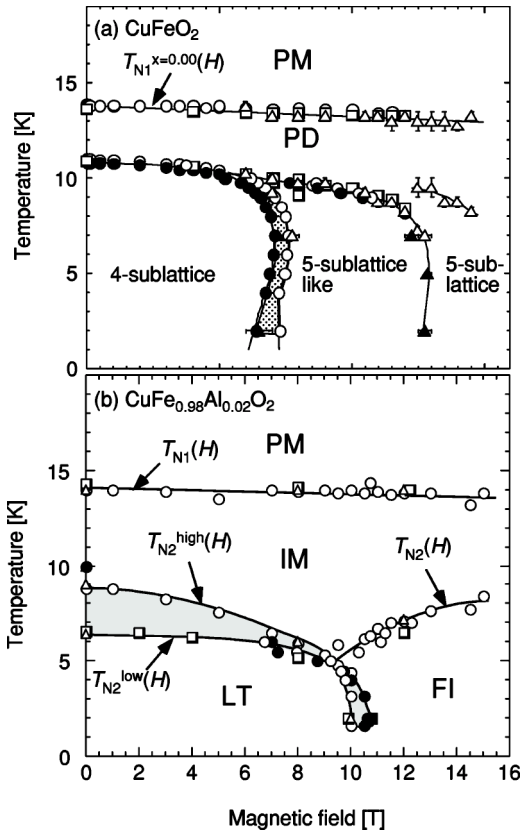

FIG. 2. (a) *H-T* magnetic phase diagrams for $CuFeO_2$ taken from Ref. 12. (Note that the region "C" in the original phase diagram was removed in the present paper, since it does not represent any magnetic phase transitions, although existence of the region C is a silent feature related to field dependence of magnetic propagation vector *q* inside five-sublattice-like phase.) (b) *H-T* magnetic phase diagrams of $CuFe_{0.98}Al_{0.02}O_2$. Anomalies found in the magnetization, neutron diffraction and specific heat measurements are depicted by circles, triangles and squares, respectively. Open and closed symbols denote the anomalies that appear with increasing and decreasing *H* or *T*, respectively. The three magnetically ordered states, intermediate-temperature, low-temperature and field-induced states, are represented by IM, LT and FI, respectively. Shading denotes the coexistence region that will be described in Sec. III C 2.

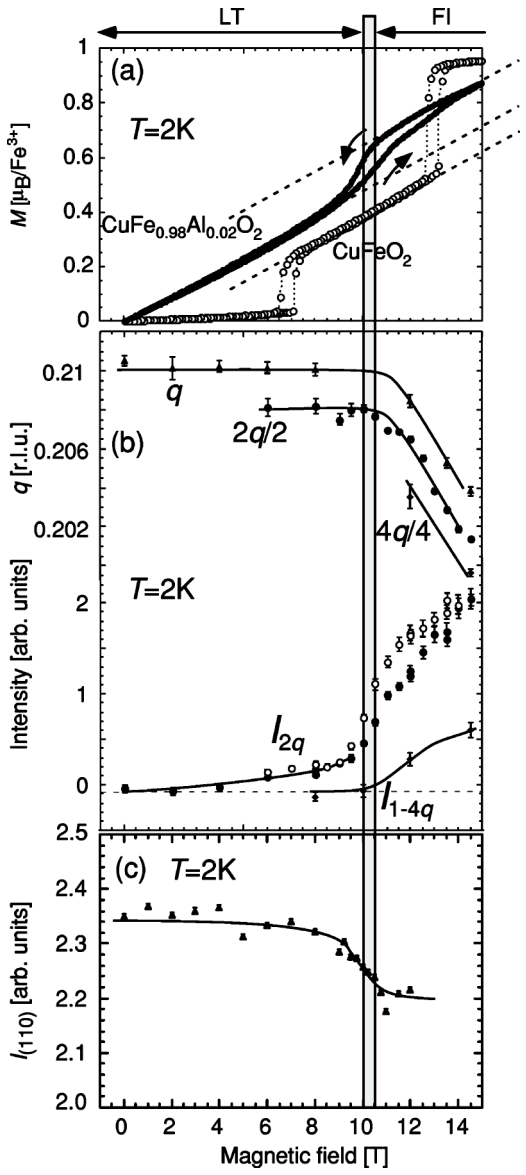

FIG. 3. (a) *M-H* curve at $T=2$ K for $CuFe_{0.98}Al_{0.02}O_2$ and $CuFeO_2$ is depicted by closed and open symbols, respectively. (b) Magnetic field dependencies of the propagation wave number *q* and of integrated intensity of the 2*q* and 4*q* reflection at $T=2$ K. To compare the field variation of 2*q* and 4*q* with that of *q* directly, we plotted the field variation of $2q/2$ and $4q/4$. Closed and open symbols are used for increasing and decreasing magnetic fields, respectively. (c) The magnetic field dependence of integrated intensity of the (1 1 0) nuclear Bragg reflection at $T=2$ K.

the incommensurate noncollinear magnetic structure inferred for the five-sublattice-like state in our previous diffraction study.[12] With these results for $CuFeO_2$, we can discuss the magnetization curve for $CuFe_{0.98}Al_{0.02}O_2$. As shown by the closed symbols in Fig. 3(a), the magnetization curve shows a discontinuous change at $H\sim 10$ T with hysteresis, corresponding to the magnetic phase transition from the LT state to the FI state. Figure 3(a) also shows that the magnetization plateaus of the commensurate states seen in $CuFeO_2$ entirely vanish in $CuFe_{0.98}Al_{0.02}O_2$. Moreover, as shown by the broken lines in Fig. 3(a), the gradient of the magnetization curves in the LT state and the FI state is almost equal to that of the incommensurate five-sublattice-like state ($7\ \mathrm{T}\leqslant H\leqslant 13$ T), implying that the spin orientations in the two states of $CuFe_{0.98}Al_{0.02}O_2$ continuously change with varying magnetic field. In fact, the present neutron diffraction data suggest that incommensurate magnetic structures are realized in both states, which will be discussed in the next section. Consequently, we found that the strong Ising anisotropy in $CuFeO_2$ is significantly reduced by the substitution of a small amount of nonmagnetic Al^{3+} impurity for Fe^{3+}. In addition, the disappearance of the quasi-Ising character in zero-field[15] certainly extends to finite magnetic fields.

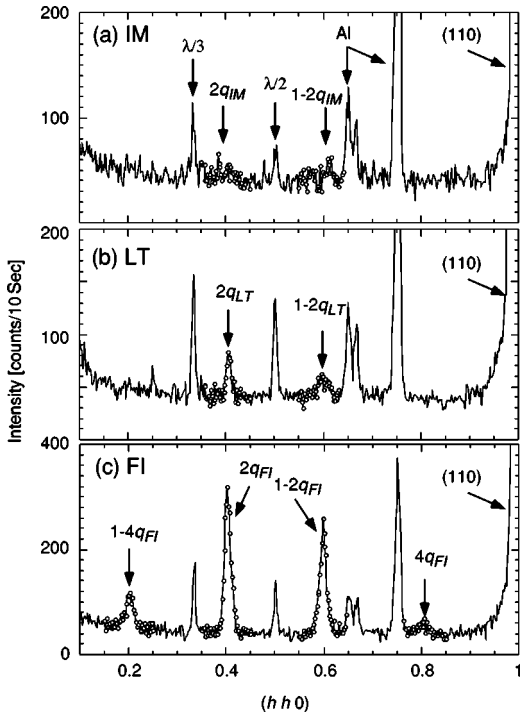

FIG. 4. Typical diffraction profiles of (hh 0) reciprocal lattice scans in (a) IM phase (H=12 T, T=11 K), (b) LT phase (H=8 T, T=2 K) and (c) FI phase (H=14.5 T, T=2 K) of $CuFe_{0.02}Al_{0.02}O_2$. Note that considering the temperature and field variation of the wave number as shown in Figs. 3(b), 5, and 6, we indexed $2q$ and $4q$ to the observed magnetic Bragg reflections. Several peaks are contamination peaks as labeled in (a).

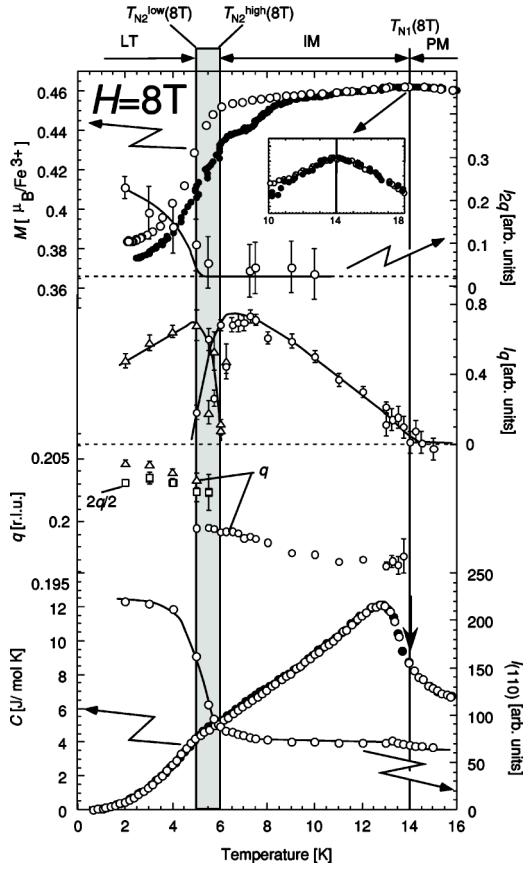

FIG. 5. Temperature dependences at H=8 T of magnetization, integrated intensities of ($2q$ $2q$ 0) and ($1-q$ $-1+2q$ 0), the propagation wave number q, integrated intensities of (1 1 0) nuclear peaks and specific heat of $CuFe_{0.98}Al_{0.02}O_2$. To compare the temperature variation of $2q$ with that of q, we show the temperature variation of $2q/2$. Open and closed symbols are used for decreasing and increasing temperature processes, respectively.

B. Magnetically ordered states

1. Low-temperature (LT) state

In the zero-field experiments, the three magnetic Bragg reflections indexed as $(q_{\mathrm{LT}}\ q_{\mathrm{LT}}\ \frac{3}{2})$, $(q'_{\mathrm{LT}}\ q'_{\mathrm{LT}}\ \frac{3}{2})$ and $(\frac{1}{2}-q'_{\mathrm{LT}}\ \frac{1}{2}-q'_{\mathrm{LT}}\ \frac{3}{2})$ were observed in the LT state. Since the wave number $q_{\mathrm{LT}}\sim 0.21$ is very close to $q'_{\mathrm{LT}}\sim 0.21$, the q_{LT} reflection and the q'_{LT} reflection were not experimentally separable. Besides, the q_{LT} reflection is dominant in the LT state. In the present high field experiment, therefore, we concentrated on investigating the dominant q_{LT} reflection, because the q'_{LT} reflection and the $(\frac{1}{2}-q'_{\mathrm{LT}})$ reflection were considered to be so small that they cannot be detected in the setup restricted to the (hk0) zone.

As seen in the typical diffraction profile of the (h h 0) scan shown in Fig. 4(b), weak magnetic Bragg reflections indexed as ($2q_{\mathrm{LT}}$ $2q_{\mathrm{LT}}$ 0) and ($1-2q_{\mathrm{LT}}$ $1-2q_{\mathrm{LT}}$ 0) were observed, where the integrated intensity of the $2q_{\mathrm{LT}}$ reflection, $I_{2q_{\mathrm{LT}}}$, is small but systematically increases with increasing magnetic field, as shown in Fig. 3(b). The wave number $q\sim 0.21$ is almost independent of the magnetic field and the temperature, as shown in Figs. 3(b) and 5. Figure 5 also shows that the integrated intensity of the (1 1 0) nuclear peak, $I_{(110)}$, increases rapidly below $T_{N2}^{\mathrm{high}}(8T)$, as was also seen in the zero-field study.[15] This situation was also observed earlier in the case of $CuFeO_2$.[8] This is because the extinction effect is reduced by the anisotropic variation of the crystal mosaicity, as was discussed in our previous reports.[8,12]

Consequently, we can infer from these experimental facts that the zero-field magnetic structure characterized by the three wave numbers, q_{LT}, q'_{LT} and $\frac{1}{2}-q'_{\mathrm{LT}}$, extends to finite magnetic fields up to $H\sim 10$ T with the $2q_{\mathrm{LT}}$ component.

2. Field-induced (FI) state

In the FI state, as seen in the typical diffraction profile of the (hh0) scan shown in Fig. 4(c), four magnetic Bragg reflections were observed at incommensurate positions ($1-4q_{\mathrm{FI}}$ $1-4q_{\mathrm{FI}}$ 0), ($2q_{\mathrm{FI}}$ $2q_{\mathrm{FI}}$ 0), ($1-2q_{\mathrm{FI}}$ $1-2q_{\mathrm{FI}}$ 0) and ($4q_{\mathrm{FI}}$ $4q_{\mathrm{FI}}$ 0). Figure 3(b) shows that at 2 K, with increasing magnetic field from the LT state, I_{2q} and I_{1-4q} increase rapidly, and the wave number starts to deviate from that of the LT state at $H\sim 10$ T. As seen in Fig. 3(c), this phase transition from the LT state to the FI state is also found in the change in $I_{(110)}$. As was seen in the case of the LT state, Fig. 6 shows that $I_{(110)}$ increases rapidly below $T_{N2}(12\ \mathrm{T})$ ~ 6.5 K due to the reduction in the extinction effect caused by the variation of crystal mosaicity. In addition, Fig. 6 shows that the magnetization, I_{2q}, the wave number $2q/2$ and

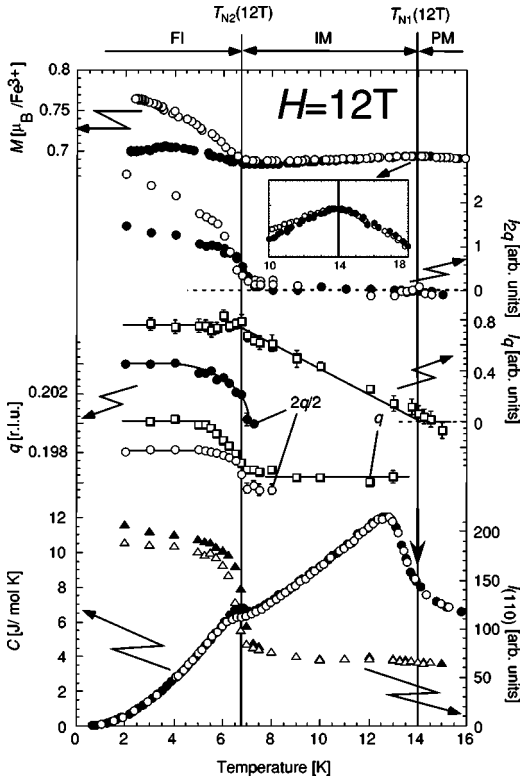

FIG. 6. Temperature dependencies at $H=12$ T of magnetization, integrated intensities of $(2q\ 2q\ 0)$ and $(1-q\ -1+2q\ 0)$ reflections, the propagation wave number q, integrated intensities of (1 1 0) nuclear peaks and specific heat of $CuFe_{0.98}Al_{0.02}O_2$. To compare the temperature variation of $2q$ with that of q, we show the temperature variation of $2q/2$. Open and closed symbols are used for decreasing and increasing temperature processes, respectively.

$I_{(110)}$ are history dependent below $T_{N2}(12\ \mathrm{T})$, which is generally observed in dilute antiferromagnets under a magnetic field. It should be noted that no thermal hysteresis was observed for the temperature variation of the specific heat reflecting the energy fluctuation. Consequently, the commensurate five-sublattice magnetic structure seen in $CuFeO_2$ entirely vanishes, and an incommensurate magnetic structure, distorted by the magnetic field, with a $2q$ component and a $4q$ component appears in the FI state.

3. Intermediate-temperature (IM) state

In the previous zero-field experiments,[15] we suggested that the magnetic structure of the IM state is different from the sinusoidally amplitude-modulated magnetic structure with collinear moments along the c axis in the PD state of $CuFeO_2$.[8] In the present (and previous[12]) high-field diffraction experiments, detailed magnetic structure determination was not performed since the experimental setup only allowed for the investigation of the $(hk0)$ zone. Nevertheless, differences between the IM state and the PD state can be studied by looking at how the higher harmonics are induced with increasing magnetic field. In the typical $(hh0)$ scan shown in Fig. 4(a), magnetic reflections with higher harmonics, such as the $2q_{\mathrm{IM}}$ reflection, were not observed within experimental accuracy at the positions expected from the observed q_{IM}

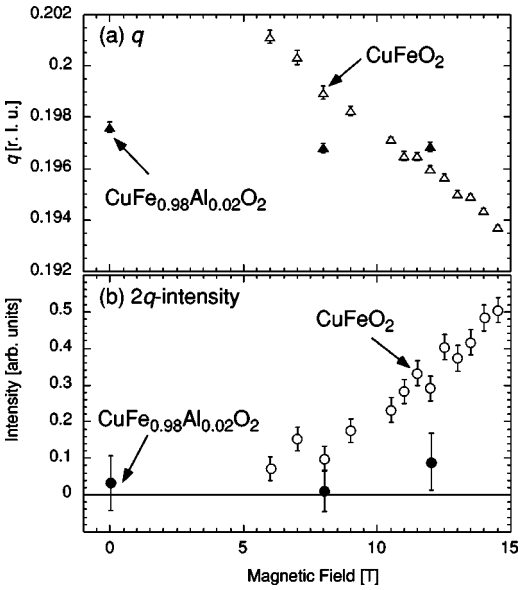

FIG. 7. Magnetic field dependencies of (a) the propagation wave number q, and (b) the integrated intensities of the $(2q\ 2q\ 0)$ magnetic Bragg reflections. Closed and open symbols are used for the IM state ($T=11$ K) of $CuFe_{0.98}Al_{0.02}O_2$ and the PD state ($T=12$ K) of $CuFeO_2$, respectively. Note that $I_{2q_{\mathrm{IM}}}$ was estimated by integrating the data around the position expected by the q_{IM} reflection, after subtracting the background data. To compare $I_{2q_{\mathrm{IM}}}$ with $I_{2q_{\mathrm{PD}}}$, these intensities were normalized to the (110) nuclear intensity.

reflection with $q_{\mathrm{IM}}\sim 0.196$ in 12 T. The fundamental wave number q_{IM} and the integrated intensity, $I_{q_{\mathrm{IM}}}$, are almost independent of the magnetic field for the IM state, as shown in Fig. 7. On the other hand, in the PD state, the integrated intensity of $2q_{\mathrm{PD}}$ reflections, $I_{2q_{\mathrm{PD}}}$, increases systematically and the wave number q_{PD} varies gradually with increasing magnetic field, as shown in Fig. 7. Consequently, in these experiments, the difference between the IM state and the PD state was clearly seen in the higher harmonics induced by increasing the magnetic field. It should be noted that the magnetization curve in both states increases linearly with increasing magnetic field.

C. Magnetic phase boundaries

1. Magnetic phase transition from para to IM

As shown in the insets in Figs. 5 and 6, a small peak anomaly in magnetization without hysteresis was observed at $T_{N1}(8\ \mathrm{T})\sim T_{N1}(12\ \mathrm{T})\sim 14$ K. This corresponds to the second-order magnetic phase transition from the paramagnetic (PM) state to the IM state. Such a transition was similarly seen in $CuFeO_2$ at $T_{N1}^{x=0.00}(H)$.[10] Figures 5 and 6 also show that the $I_{q_{\mathrm{IM}}}$ starts to increase below $T_{N1}(8\ \mathrm{T})$ and $T_{N1}(12\ \mathrm{T})$; at the same time, a small anomaly in the specific heat was found at $T_{N1}(8\ \mathrm{T})$ and $T_{N1}(12\ \mathrm{T})$ as shown by arrows in Figs. 5 and 6, in contrast to the distinct lambda-type anomaly in specific heat in $CuFeO_2$ at $T_{N1}^{x=0.00}(H)$.[10] Consequently, $T_{N1}(H)$ remains almost unchanged from $T_{N1}^{x=0.00}(H)$ as seen in Fig. 2, apart from a slight increase in $T_{N1}^{x=0.00}(H)$

due to the partial release of the spin frustration, as was discussed in the previous powder study.[5]

2. Magnetic phase transition from IM to LT

The transition temperature $T_{N2}^{\mathrm{high}}(0\ \mathrm{T})$ and $T_{N2}^{\mathrm{low}}(0\ \mathrm{T})$ separating the IM state and the LT state were defined in the zero-field experiments[15] as the respective temperatures where, with decreasing temperature, the temperature variation of magnetic susceptibility along the *c* axis starts to deviate downward from that perpendicular to the *c* axis, and where the specific heat shows a dull peak. The temperature region between $T_{N2}^{\mathrm{high}}(0\ \mathrm{T})$ and $T_{N2}^{\mathrm{low}}(0\ \mathrm{T})$ was identified as the *coexistence region* where $I_{q_{\mathrm{IM}}}$ coexists with $I_{q_{\mathrm{LT}}}$.

Figure 5 shows that with decreasing temperature from the IM state at $H=8$ T, the magnetization starts to fall at $T_{N2}^{\mathrm{high}}(8\ \mathrm{T})\sim 6$ K, and the specific heat shows a dull peak at $T_{N2}^{\mathrm{low}}(8\ \mathrm{T})\sim 5$ K. The $I_{q_{\mathrm{IM}}}$ starts to decrease at $T_{N2}^{\mathrm{high}}(8\ \mathrm{T})$ and vanishes at $T_{N2}^{\mathrm{low}}(8\ \mathrm{T})$; at the same time, $I_{q_{\mathrm{LT}}}$ starts to increase at $T_{N2}^{\mathrm{high}}(8\ \mathrm{T})$, where the wave number q shows a discontinuous change in the coexistence region. $I_{(110)}$ also starts to increase at $T_{N2}^{\mathrm{high}}(8\ \mathrm{T})$. Consequently, the magnetic phase transition from the IM state to the LT state through the coexistence region was also found at $H=8$ T, as was seen in the zero magnetic field. The coexistence region in the zero magnetic field becomes gradually narrower with increasing magnetic field, and, as illustrated in Fig. 2(b), converges to the triple point where the three states meet.

3. Magnetic phase transition from IM to FI

At the phase boundary between the IM and the FI states, starting from the IM state at 12 T, a decrease in temperature produces a magnetic phase transition to the FI state at $T_{N2}(12\ \mathrm{T})\sim 6.5$ K without the coexistence region. As Fig. 6 makes apparent, the temperature variation of the magnetization exhibits a local minimum, and the wave number q changes continuously at $T_{N2}(12\ \mathrm{T})$, which is entirely different from the case in which $H=8$ T. At the same time, a dull peak in the specific heat appears at $T_{N2}(12\ \mathrm{T})$, and $I_{2q_{\mathrm{FI}}}$ also starts to rise rapidly below $T_{N2}(12\ \mathrm{T})$. Collecting the transition temperatures from the IM to the FI state in several magnetic fields, we found that $T_{N2}(H)$ systematically increases from the triple point with increasing magnetic field as shown in Fig. 2(b); in contrast, Fig. 2(a) demonstrates that all the transition temperatures in $CuFeO_2$ systematically decrease with increasing magnetic field.

IV. DISCUSSION AND CONCLUSIONS

We have performed neutron diffraction, magnetization and specific heat measurements on the triangular lattice antiferromagnet $CuFe_{0.98}Al_{0.02}O_2$, using single-crystal samples. The experimental findings are briefly summarized below.

First, the shape of the *H-T* magnetic phase diagram is completely modified from that of $CuFeO_2$; the character of the triple-point where the three states meet differs between $CuFeO_2$ and $CuFe_{0.98}Al_{0.02}O_2$. This strongly suggests that a small amount of nonmagnetic impurity modifies the thermodynamic properties of $CuFeO_2$.

Second, the results of the magnetization measurements at low temperatures for both $CuFeO_2$ and $CuFe_{0.98}Al_{0.02}O_2$ showed that the strong Ising anisotropy seen in $CuFeO_2$ is significantly reduced by the substitution. In addition, the disappearance of the quasi-Ising character in the zero field[15] extends to a finite magnetic field. With this experimental finding, we can briefly discuss the origin of the anisotropy in $CuFeO_2$. The single ion anisotropy energy of the orbital singlet Fe^{3+} is so small that the quasi-Ising magnetic orderings in $CuFeO_2$ cannot be explained. Even if it is adequately strong, the single ion anisotropy should not be significantly reduced by the substitution of a small amount of nonmagnetic impurity.

Third, through the neutron diffraction experiments, we also found that the commensurate magnetic orderings seen in $CuFeO_2$ disappear, and the incommensurate magnetic orderings appear. As a ground state, instead of the collinear four-sublattice ($\uparrow\uparrow\downarrow\downarrow$) magnetic structure in $CuFeO_2$, the incommensurate magnetic structure characterized by the three wave numbers, q_{LT}, q'_{LT} and $\frac{1}{2}-q'_{\mathrm{LT}}$, may extend to a finite magnetic field up to $H\sim 10$ T. The field-induced state with the commensurate five-sublattice magnetic structure ($\uparrow\uparrow\uparrow\downarrow\downarrow$) in $CuFeO_2$ vanishes, and the incommensurate magnetic structure, distorted by the magnetic field, with second and fourth higher harmonics, is realized. In addition, in the IM state, the magnetic structure that is different from the collinear sinusoidally amplitude-modulated structure with the magnetic moments along the *c* axis in the PD state of $CuFeO_2$ extends to a finite magnetic field without higher harmonics.

With the above three findings, we recently performed inelastic neutron scattering experiments on $CuFeO_2$ and $CuFe_{0.98}Al_{0.02}O_2$. Reflecting the differences in the thermodynamic properties for the two samples, the spin-wave dispersion relations are also quite different from each other. While a spin-wave dispersion curve without an energy gap was obtained for $CuFe_{0.98}Al_{0.02}O_2$, an unusual dispersion curve with an energy gap, whose bottom positions do not correspond to the magnetic Bragg point for the four-sublattice ground state, was obtained for $CuFeO_2$.[17]

We should mention other chemical impurity effects on the $CuFeO_2$ magnetic system. Hasegawa *et al.* have reported that the low transition temperature, T_{N2}, of $CuFeO_2$ depends on the oxygen defect concentration.[14] They concluded that Fe^{2+} or Cu^{2+} are induced by oxygen deficiency or an excess of oxygen, respectively. Although the content of the divalent ions as an "impurity" was 17% maximum, all of their samples maintained the four-sublattice state. This is in contrast to our results wherein the four-sublattice state disappeared with only 2% substitution of nonmagnetic Al^{3+} impurity.

Also, we have to state here that our previous specific heat data in zero magnetic field for $CuFeO_2$[9] were inconsistent with the data of Petrenko *et al.*[11] and Takeda *et al.*[4]: although the data of two groups showed a sharp peak corresponding to a large latent heat at T_{N2}, our data did not show such a peak at T_{N2}. However, reviewing our previous data carefully, we found that we missed a large sharp peak corresponding to a

latent heat at very narrow first-order phase transition point T_{N2}, which is almost quantitatively consistent with the data of Petrenko *et al.* Therefore, we add here that, as a result of the substitution of a small amount of nonmagnetic impurity, the large sharp peak, observed in the specific heat for $CuFeO_2$, disappears, reflecting the dramatic changes in the thermodynamic properties between $CuFeO_2$ and $CuFe_{0.98}Al_{0.02}O_2$.

In conclusion, we have obtained the *H-T* magnetic phase diagram for $CuFe_{0.98}Al_{0.02}O_2$ using neutron diffraction, magnetization and specific heat measurements. The *H-T* phase diagram is entirely modified from that of $CuFeO_2$ by the substitution of a small amount of nonmagnetic Al^{3+} impurity for Fe^{3+}, suggesting that the quasi-Ising character seen in $CuFeO_2$ disappears and the Heisenberg character of the orbital singlet Fe^{3+} is retrieved.

ACKNOWLEDGMENTS

Neutron diffraction experiments at BENSC were performed in accordance with the proposal (PHY-01-1035) for the beam time in 2001/II, where N.T. was supported by Hahn–Meitner Institut. This work was partly supported by Grants-in-Aid for Scientific Research from the Japan Society for the Promotion of Science.

*Electronic address: terada@nsmsmac4.ph.kagu.tus.ac.jp

[1] M. F. Collins and O. A. Petrenko, Can. J. Phys. **75**, 605 (1997).
[2] M. Mekata, N. Yaguchi, T. Takagi, T. Sugino, S. Mitsuda, H. Yoshizawa, N. Hosoito, and T. Shinjo, J. Phys. Soc. Jpn. **62**, 4474 (1993).
[3] Y. Ajiro, T. Asano, T. Takagi, M. Mekata, H. Aruga Katori, and T. Goto, Physica B **201**, 71 (1994).
[4] K. Takeda, K. Miyake, M. Hitaka, T. Kawae, N. Yaguchi, and M. Mekata, J. Phys. Soc. Jpn. **63**, 2017 (1994).
[5] S. Mitsuda, Y. Matsumoto, T. Wada, K. Kurihara, Y. Urata, H. Yoshizawa, and M. Mekata, Physica B **213-214**, 194 (1995).
[6] Y. Ajiro, K. Hanasaki, T. Asano, M. Mekata, H. Aruga Katori, and T. Goto, J. Phys. Soc. Jpn. **64**, 3643 (1995).
[7] T. Fukuda, H. Nojiri, M. Motokawa, T. Asano, M. Mekata, and Y. Ajiro, Physica B **246-247**, 569 (1998).
[8] S. Mitsuda, N. Kasahara, T. Uno, and M. Mase, J. Phys. Soc. Jpn. **67**, 4026 (1998).
[9] S. Mitsuda, T. Uno, M. Mase, H. Nojiri, K. Takahashi, M. Motokawa, and M. Arai, J. Phys. Chem. Solids **60**, 1249 (1999).
[10] S. Mitsuda, M. Mase, T. Uno, H. Kitazawa, and H. Aruga Katori, J. Phys. Soc. Jpn. **69**, 33 (2000).
[11] O. A. Petrenko, G. Balakrishnan, M. R. Lees, D. Mck. Paul, and A. Hoser, Phys. Rev. B **62**, 8983 (2000).
[12] S. Mitsuda, M. Mase, K. Prokes, H. Kitazawa, and H. Aruga Katori, J. Phys. Soc. Jpn. **69**, 3513 (2000).
[13] Y. Oohara, M. Mekata, T. Morishita, K. Kakurai, M. Nishi, T. R. Zhao, and H. Takei, J. Phys. Soc. Jpn. **70**, 3031 (2001).
[14] M. Hasegawa, M. I. Batrashevich, T. R. Zhao, H. Takei, and T. Goto, Phys. Rev. B **63**, 184437 (2001).
[15] N. Terada, S. Mitsuda, S. Suzuki, M. Fukuda, T. Kawasaki, T. Nagao, and H. Aruga Katori, J. Phys. Soc. Jpn. **73**, 1442 (2004).
[16] T. R. Zhao, M. Hasegawa, and H. Takei, J. Cryst. Growth **166**, 408 (1996).
[17] N. Terada, S. Mitsuda, Y. Oohara, H. Yoshizawa, and H. Takei, J. Magn. Magn. Mater. **272–276S**, E997 (2004).